The Role of Indian Ocean Warming on Extreme Rainfall in Central China During Early Summer 2020: Without El Niño Influence

Yinan Cai
South China Sea Institute of Oceanology Chinese Academy of Sciences
Zesheng Chen
South China Sea Institute of Oceanology Chinese Academy of Sciences
Yan Du (duyan@scsio.ac.cn)
South China Sea Institute of Oceanology Chinese Academy of Sciences https://orcid.org/0000-0002-7842-0801

Research Article

Keywords: extreme rainfall, the Indian Ocean warming, WNPAC, water vapor transport

Posted Date: August 3rd, 2021

DOI: https://doi.org/10.21203/rs.3.rs-748847/v1

Version of Record: A version of this preprint was published at Climate Dynamics on February 13th, 2022.
See the published version at https://doi.org/10.1007/s00382-022-06165-9.

Abstract

This study investigates the role of water vapor transport and sea surface temperature (SST) warming in the tropical Indian Ocean (TIO) on the heavy rainfall in central China during boreal early summer. In the past four decades, four significant rainfall events, in 1983, 1998, 2016, and 2020, occured in central China and caused severe floods, in which the year 2020 has the most extreme event. All four events are associated with significant TIO SST warming, associated with a strong and westward extending anomalous anticyclone on the western North Pacific (WNPAC). The anomalous winds in the northwestern flank of the WNPAC bring excess water vapor into central China. The water vapor, mainly carried from the central tropical Pacific, converges in central China and result in heavy rainfall. A theory of regional ocean-atmosphere interaction can well explain the processes, called the Indo-Western Pacific Ocean Capacitor (IPOC) effect. The WNPAC is usually associated with strong El Niño-Southern Oscillation (ENSO), except for the 2020 case. The 2020 event is extraordinary, without ensuring El Niño occurred in the previous winter. In 2020, the significant TIO warming sustained the anomalous WNPAC, inducing the most significant extreme rainfall event in central China. This study reveals that the IPOC effect can dramatically influence the East Asian climate even without involving the ENSO in the Pacific.

1 Introduction

Boreal summer is the rainy season for China. During early summer (May-June-July, MJJ), warm and moist southwesterly winds, originated from the Indian Ocean, the South China Sea, and the Western Pacific, supply abundant water vapor to central China (Fig. 1a; Sampe and Xie, 2010), one of the most populated regions in China, ranged from 106.25°E-121.25°E, 26.25°N-33.75°N in this study (the red box in Fig. 1a). The rainfall in central China has strong interannual variability (Fig. 1b) and is greatly influenced by the El Niño-Southern Oscillation (ENSO) (Huang and Sun 1992, Wu et al., 2003; Wang et al., 2013; Chen et al., 2017; 2019). For example, during the decay phase of an El Niño event, a significant low-level anticyclone maintains over the western North Pacific (WNPAC), indicating the western Pacific Subtropical High (WPSH) is more intense and southward compared to its climatology (Lu and Dong, 2001; Gao et al., 2019). More water vapor is transported into central China due to the anomalous southwesterly winds in the northwestern flank of the WNPAC, thus increasing the rainfall in central China (Chen 2002; Ding 1992; Ding and Wang 2008; Zhou and Yu, 2005). The previous study revealed that a basin-wide sea surface temperature (SST) warming in the tropical Indian Ocean (TIO) always follows an El Niño event and peaks in the boreal spring (e.g., Klein 1999; Alexander et al., 2002; Chiang and Sobel, 2002; Du et al., 2009; Xie et al., 2016). The TIO warming plays an important role in sustaining the WNPAC when the El Niño turns to the decay phase (e.g., Yang et al., 2007; Xie et al., 2016; Chen et al., 2018).

The anomalous rainfall in central China can largely affect socioeconomic activity and influence millions of people. Zhou et al. (2021) reported that the June-July rainfall in 2020 was twice the mean of 1981–2010. It caused severe floods lashing Yangtze River Valley and Huai River Valley (Ding et al., 2021). By 22 July 2020, more than 45.5 million people were affected, and 142 people were dead or missing, with a direct economic loss of 116 billion yuan (16.6 billion US dollars) (Wei et al., 2020). Figure 1b shows the

time series of rainfall anomalies in central China during early boreal summer. Four significant rainfall events, which exceed one standard deviation of rainfall anomaly, occurred in 1983, 1998, 2016, and 2020. The 2020 rainfall event was extremely strong, with its rainfall anomaly exceeded three standard deviations, making a historical record since 1979 (Fig. 1b) and even 1961 (Ding et al., 2021). Many factors may contribute to the 2020 extreme rainfall in central China (e.g., Takaya et al., 2020; Ding et al., 2021; Zhou et al., 2021; Zheng and Wang, 2021). Ding et al. (2021) reported that the East Asian monsoon circulation system, including the high-level westerly jet, the low-level southwesterly jet, and WPSH, featured a quasi-biweekly oscillation, all contributing to this extreme event. Besides, the atmospheric circulation pattern in the middle to high latitudes facilitated the cold air intrusions to the central China region, making an extraordinary contribution (Ding et al., 2021). Takaya et al. (2020) proposed that the Indian Ocean warming enhanced the 2020 summer rainfall in East Asia and regarded the extreme Indian Ocean Dipole (IOD) in 2019 as the cause. Zhou et al. (2021) further highlighted the role of 2019 IOD in the historic Yangtze flooding in 2020.

Water vapor is the basis of local precipitation, influenced by the atmospheric circulation through advection and vertical transport (Zhou et al. 2005; Sherwood et al. 2010; Zhu et al. 2011). Regional water vapor supply arises mainly from two sources: local evaporation and external moisture advection. On the continent, Benton et al. (1950) showed that even local evaporation is significant, the external moisture advection contributes the majority of rainfall. As the abnormal water vapor continuously enters the sink region, heavy rainfall can be formed (Trenberth et al., 2003). Water vapor transport is vital for determining the rainfall pattern of China (Simmonds et al. 1999; Ninomiya and Kobayashi 1998; Ding and Sun 2001). For four significant rainfall events in central China in 1983, 1998, 2016, and 2020, the origin of the water vapor and the cause of such water vapor transport patterns are not always the same. This motivates us to distinguish the difference, especially for the 2020 event, from the aspect of water vapor transport. This study found that not like the other three events, no strong El Niño conditions occurred in the central to eastern equatorial Pacific in the previous winter of 2020. Only a weak warm state appeared in the central-western tropical Pacific. Our research investigates the 2020 case and demonstrates the greatly important role of TIO SST warming even without ensuring El Niño in the Pacific.

The rest of the study is organized as follows. Section 2 describes the dataset and methods utilized in this work. Section 3 analyzes the water vapor transport associated with four significant rainfall events. Section 4 explores the direct impact of WNAPC. Section 5 discusses the IPOC effect on extreme rainfall in central China during early summer 2020 in detail. Section 6 summarizes major points and provides further discussions.

2. Data And Methodology

In this study, monthly mean atmospheric data, including geopotential wind, sea level pressure, and specific humidity, are from the fifth generation European Centre for Medium-Range Forecasts (ECMWF) reanalysis (ERA5) (https://cds.climate.copernicus.eu) (Hersbach et al. 2019a, 2019b). The horizontal resolution of the ERA5 datasets is 0.75°×0.75°. Global Precipitation Climatology Project (GPCP)

precipitation data are provided by the NOAA/OAR/ESRL PSL, Boulder, Colorado, USA, from their website at https://psl.noaa.gov/data/gridded/data.gpcp.html. The sea surface temperature (SST) data on a 1°×1° grid are derived from the NOAA/OAR/ESRL PSL, Boulder, Colorado, USA, from their website at https://www.psl.noaa.gov/data/gridded/data.noaa.oisst.v2.html (Reynolds et al. 2002). All above data are available during the period 1979–2020. Anomalies are calculated relative to the climatological seasonal cycle based on the period 1979–2020. The Niño3.4 SST index is also used in this study, which is defined as the SST anomaly in the Niño3.4 region (170°W-120°W, 5°S-5°N). This index is available from NOAA/ESRL, updated weekly from 1982 to 2020 (https://stateoftheocean.osmc.noaa.gov/sur/pac/nino34.php). In the present study, the statistical significance of the composite anomalies is assessed by a student's *t* test.

The ERA5 monthly mean vertically integrated zonal and meridional water vapor flux are defined as follows.

$$\vec{Q} = \int_{p_t}^{Ps} \left(\vec{V} \bullet q \right) dp / g \quad (1)$$

p_s is the surface atmospheric pressure, $\vec{V}$ is the zonal and meridional wind, q is the specific humidity, g is the gravitational acceleration. p_s and p_t are the pressures at the ground surface and top of the troposphere, respectively. Since moisture content above 200 hPa can be negligible (Trenberth 1991), the vertically integrated water vapor flux is integrated from 1000 hPa to 200 hPa in our study.

The divergence of vertically integrated water vapor flux can be expressed as:

$$Div = \nabla \bullet \vec{Q} = \frac{\partial \vec{Q}_\lambda}{\partial x} + \frac{\partial \vec{Q}_\phi}{\partial y} \quad (2)$$

Div and $\nabla \bullet \vec{Q}$ are the divergence, $\vec{Q}_\lambda$ is vertically integral of zonal water vapor flux and $\vec{Q}_\phi$ is vertically integral of meridional water vapor flux.

We integrate the water vapor flux across each line segment along the boundaries of central China. The equation (Richter and Xie 2010) is

$$tr = \int_0^l \vec{Q} dl \quad (3)$$

Where tr is the moisture transport across the boundary, and the unit is Sverdrup (symbol: Sv), with 1 Sv equal to $10^6 \mathrm{m}^3 \cdot \mathrm{s}^{-1}$, l is position along the boundary.

3 Water Vapor Transport Associated With Significant Rainfall Events

To illustrate the relationship between water vapor supply, ascending motion, and rainfall over central China, average mean rainfall, net regional water vapor budget, and p-velocity at 500 hPa (multiplied by −1, −ω500) anomalies over central China are displayed in Fig. 2. The early summer rainfall anomalies over central China show remarkably interannual variation and coincide well with the water vapor budget and −ω500 (Fig. 2). In general, the year-to-year pulse of the rainfall anomalies is consistnet with the change of the water vapor budget and −ω500. The rainfall and net water vapor budget are highly correlated, and their correlation coefficient (r) is 0.75. The correlation coefficient between rainfall and −ω500 is slightly higher ($r = 0.79$). All these coefficients are statistically significant at the 95% confidence level. In four significant rainfall events (defined in Fig. 1b; 1983, 1998, 2016, and 2020), positive rainfall is corresponding to positive net water vapor budget and −ω500, which indicates that the water vapor supply and local vertical motion are important for the rainfall in central China. It is reasonable to investigate the possible mechanisms governing heavy rainfall over central China from the aspect of external water vapor transport.

The vertically integrated water vapor transport flux (WVF) and the divergence for climatological conditions are presented in Fig. 3a. During MJJ, three branches of water vapor are converyed into central China. The first one is water vapor from the northern Indian Ocean, which originates in the southern Indian Ocean. The second one is the warm and moist water vapor transported from the Southern Hemisphere and the South China Sea, and the third one is carried from the tropical western Pacific Ocean. Warm and moist water vapor meets and converges over central China (Fig. 3a). The western and southern boundaries of central China are the main input boundaries. About 0.04 Sv and 0.23 Sv water vapor are brought into the region, respectively. The eastern boundary is the main outflow boundary (0.13 Sv). The water vapor carried out through the eastern boundary is much stronger than that via the northern boundary (0.05 Sv). In Fig. 3a, strong convergence regions also include western India and western South Asia, where the external water vapor supply is strong. As a result, more precipitation appears over these areas than in other places (Fig. 1a). For four significant early summer rainfall events, composites of water vapor flux and divergence anomalies are shown in Fig. 3b. Excess water vapor is transported westwards from the tropical western Pacific to the Bay of Bengal and converges. Meanwhile, extra water vapor is transported into central China through a northeastward water vapor pathway and converged there (Fig. 3b). The anomalous water vapor supply to central China has two branches, from the tropical western Pacific and the north Indian Ocean. Anomalous moisture divergences also appear in South Asia and the tropical western Pacific during significant rainfall events.

Figure 3 indicates that the southern boundary is the main water vapor input boundary, playing an important role in the rainfall of central China. The relationship between rainfall anomalies of central China and water vapor input anomalies through the southern boundary is quantified in Fig. 4. Results showed that rainfall anomalies coincide very well with entering water vapor anomalies in the south ($r = 0.59$). When central China receives more rainfall, more water vapor is transported through its southern boundary. In four significant early summer rainfall cases, water vapor entered through the southern

boundary are particularly strong, all exceed one standard deviation, increasing about 30% (0.07Sv, 1983), 39% (0.09Sv, 1998), 22% (0.05Sv, 2016), and 43% (0.10Sv, 2020) over the mean state, respectively (Fig. 4). It suggests that during four significant rainfall events, extra water vapor is carried through the southern boundary by the northeastward water vapor path, then converges in central China and leads to heavy rainfall finally.

4 Wnpac Impacts On Extreme Rainfall

To unravel the origin of water vapor, the composite of 850 hPa wind anomalies in four significant rainfall events is displayed in Fig. 5a. During four significant rainfall events, an anomalous strong anticyclone appears over the western North Pacific (WNPAC). Strong anomalous easterly winds blow from the tropical western Pacific to the Indian Ocean, which weakens the climatological westerly winds. Meanwhile, part of anomalous easterly winds turns to northeastwards and blow to East Asia (Fig. 5a). Geopotential height anomalies at 500 hPa during four cases are shown in Fig. 5b. In four significant rainfall events, significantly increased geopotential height is observed in most regions (e.g., the tropical western Pacific, the Indian Ocean, and eastern China). The maximum enhancement appears over the western North Pacific. On the contrary, geopotential height decreases over Mongolia (Fig. 5b). The center of the WPSH is extended westward and southward compared to its climatological mean (Fig. 5b), which is consistent with the position of anomalous WNPAC (Fig. 5a). A large amount of water vapor is transported into central China by the southwesterly jet at the northwestern edge of the WPSH. It also means that the northwest flank of the WNPAC is the northeastward water vapor path mentioned in the last section.

To quantify the intensity of WNPAC, this study defines a WNPAC index, as the 850 hPa zonal wind difference between a southern region (100°E-130°E, 5°N-15°N) and a northern region (110°E-140°E, 25°N-35°N). The definition follows Huang et al. (2010), except that the northern region shifts northward. A positive (negative) WNPAC index indicates an anomalous anticyclone (cyclone) appears in the western North Pacific. The relationship between WNPAC and El Niño is shown in Fig. 6. In most El Niño events, a significant anticyclone appears in the western North Pacific during the decay phase (Fig. 6), consistent with previous studies. For four significant rainfall events, the values of the WNPAC index are positive and large, which indicates the enhanced WNPAC during these years. It is worth noting that 1983, 1998, and 2016 rainfall cases were associated with preceding strong El Niño events. However, no significant El Niño occurred in 2019/2020 winter. The WNPAC index is positively correlated with the Niño3.4 index with a correlation coefficient of 0.66. The correlation coefficient becomes slightly higher (0.69) when the 2020 event is removed. All these coefficients are statistically significant at the 95% confidence level. These results suggest that such enhanced and westward extending WNPAC supplies continuous water vapor to central China through its northwestern flank. The resultant strong converge over central China would, in turn, lead to heavy rainfall. During three significant rainfall cases, following strong El Niño events (1983, 1998, 2016), the WNPAC was highly related to El Niño. However, a strong WNPAC in 2020 occurred without El Niño. Therefore, one provoking question is what process sustained the WNPAC in 2020.

5 Ipoc Effect On 2020 Event Without El Niño

SST, 850 hPa winds, and rainfall anomalies during MJJ of three events (1983, 1998, 2016) and 2020 are compared and presented in Fig. 7. The western Pacific and the northern Pacific were warming when the southeastern Pacific was cooling in 2020, opposite the SST pattern of the other three events (Fig. 7a, c). In all significant rainfall events, the tropical Indian Ocean and the South China Sea are warming. Anomalous easterly winds blow from the tropical western Pacific to the Bay of Bengal, and an anticyclone appears on the western North Pacific (Figs. 7a, c). During four significant events, rainfall in the western North Pacific and South Asia decreased. On the contrary, more rainfall occurred over the tropical eastern Indian Ocean, East Asia, and Japan (Figs. 7b, d). In 2020, the SST warming dominated the TIO and even extended to the tropical western Pacific, while the eastern equatorial Pacific maintained a slight cooling state (Fig. 7c), the eastern equatorial Pacific SST cooling may play an important role in maintaining the WNPAC due to atmospheric Rossby wave response to its northwest (Chen et al., 2016). Induced by the TIO warming, anomalous easterly winds extended to the Arabian Sea; more rainfall occurred in the entire TIO basin in 2020 (Figs. 7c, d). According to the IPOC theory, the above processes were sustained by WNPAC (Xie et al., 2009 & 2016).

IPOC theory well explains the relationship between Indian Ocean SST warming and the western North Pacific anomalous circulation. In 2020 early summer, the TIO rainfall is the key. The rainfall and SST anomalies averaged over the TIO region are displayed in Fig. 8. Despite that, the correlation of the year-to-year fluctuation of the SST and rainfall anomalies over the TIO is not very high (r = 0.38). The positive correlation coefficient indicates the ocean SST forcing relates to rainfall in a particular year. SST of TIO has substantial interannual variation, and there are significant increasing trends for rainfall and SST since 1982 (Fig. 8, the linear fittings). For four significant rainfall events (1983, 1998, 2016, 2020), the TIO SST and rainfall anomalies are distributed above the linear trend lines, indicating that the TIO SST warming matches abnormal positive rainfall in these years (Fig. 8). The most striking feature for four significant rainfall events is the excess rainfall in the TIO forced by the intense TIO warming. Among the four cases, the 2020 event is the most significant since the TIO rainfall reaches the maximum. In recent decades, the TIO warming trend may also provide a favorable background to maintain a stronger WNPAC (Fig. 8), and the 2020 extreme rainfall in central China was a manifestation. We also find that significant TIO warming and enhanced rainfall appeared in 2010, associated with the delayed response to El Niño (Chen et al., 2016). In the summer of 2010, the TIO warming also played an essential role in maintaining the WNPAC (Figs. 6 and 8). As a result, abnormal positive rainfall appeared in central China (Fig. 1), due to the IPOC effect. Note, the WNPAC in 2010 was slightly southward, compared to the four significant rainfall events; thus, rainfall in central China was weaker.

Climatologically, in the low latitude, the zonal water vapor is transported from the northern Indian Ocean to the western Pacific, and in the middle latitude, water vapor is transported eastwards north of 30°N (Fig. 9a). In 2020 early summer, the zonal water vapor is enhanced north of 20°N, and the maximum enhancement appears around 30°N. The slight enhancement also appeared in the northern Arabian Sea. On the contrary, zonal water vapor is weakened over the Bay of Bengal, the South China Sea, and the

tropical Pacific (Fig. 9a). As a result, less water vapor from the Bay of Bengal is transported to the tropical western Pacific. More eastwards water vapor is transported through the eastern boundary of central China. Climatologically, the meridional water vapor is transported from ocean to continent in most regions (Fig. 9b). In general, the zonal water vapor transport was larger than the meridional water vapor. In 2020 early summer, excessive northward meridional water vapor was transported from the South China Sea to central China (Fig. 9b), related to enhanced and westward extending WNPAC and TIO SST warming.

6 Conclusions

This study mainly reveals that the extreme rainfall of 2020 MJJ is attributed to the IPOC effect even without involving the ENSO in the Pacific. In the past four decades, four significant rainfall events (1983, 1998, 2016, and 2020) occurred in central China, resulting in catastrophic floods. The year 2020 has the most extreme rainfall among four significant events. This study investigated the cause for the 2020 extreme rainfall from water vapor transport and TIO SST warming. In climatology, three pathways carry water vapor to central China from tropical Indian and Pacific Oceans, and the schematic representation is displayed in Fig. 10a. In the first pathway, the warm and moist water vapor is originated from the south Indian Ocean, transporting northeastwards to central China. In the second pathway, the water vapor is brought from the southern hemisphere and the South China Sea. In the third pathway, the water vapor is carried from the western Pacific (Fig. 10a). During 2020, the intense warming of the tropical Indian Ocean excited a strong and westward extending WNPAC in MJJ, coupled with the TIO SST warming (Fig. 10b). Such coupled mechanism persisted in the early summer. Meanwhile, TIO SST warming forced enhanced rainfall in the Indian Ocean basin. Excess water vapor was carried into central China mainly through the southern boundary by the northwestern flank of the WNPAC and convergence in central China, leading to record-breaking rainfall. Rainfall intensity is strengthened on the northern branch of the WNPAC. On the contrary, less rainfall appeared over the western Pacific due to the WNPAC and suppressed advection (Fig. 10b) due to the IPOC effect.

Traditionally, ENSO is a trigger of the IPOC effect. During the 1983, 1998, and 2016 cases, super El Niño happened in the previous winter. El Niño affects the southwest Indian Ocean through westward oceanic Rossby waves, which induced the southwest Indian Ocean to warm up. In turn, the SST warming yields an anti-symmetrical wind pattern over the TIO during the spring, persisting through the following summer. The second TIO SST warming excites a Matsuno-Gill-type response in tropospheric temperature, inspires a warm Kelvin wave into the western Pacific. As a result, an enhanced and westward extending WNPAC appears. Such a process is consistent with previous studies (e.g., Du et al. 2009; Kosaka et al. 2013; Wang et al. 2013; Xie et al. 2009). Unlike the other three events (1983, 1998, and 2016), no significant El Niño occurred in 2019/2020. In 2020 early summer, a strong and westward extending WNPAC was sustained by the significant TIO warming. This study reveals that the IPOC effect could be established and maintained without significant El Niño.

Declarations

Acknowledgments

This work is supported by the National Natural Science Foundation of China (41830538, 42090042), the Chinese Academy of Sciences (XDB42010305, XDA15020901, 133244KYSB20190031, ZDRW-XH-2019-2), and the Southern Marine Science and Engineering Guangdong Laboratory (Guangzhou) (GML2019ZD0303, GML2019ZD0306, 2019BT02H594), the Independent Research Project Program of State Key Laboratory of Tropical Oceanography (LTOZZ2102).

References

1. Alexander MA, Blade I, Newman M, Lanzante JR, Lau NC, Scott JD (2002) The atmospheric bridge: The influence of ENSO teleconnections on air-sea interaction over the global oceans. J Clim. 15:2205–2231. https://doi.org/10.1175/1520-0442(2002)015<2205:TABTIO>2.0.CO;2
2. Benton GS, Blackburn RT, Snead VO (1950) The role of the atmosphere in the hydrologic cycle. Eos, Transactions American Geophysical Union 31.1:61–73. https://doi.org/10.1029/TR031i001p00061
3. Chen J, Wang X, Zhou W, Wang C, Xie Q, Li G, Chen S (2018) Unusual rainfall in southern China in decaying August during extreme El Niño 2015/16: Role of the western Indian Ocean and north tropical Atlantic SST. J Clim 31.17:7019–7034. https://doi.org/10.1175/JCLI-D-17-0827.1
4. Chen W (2002) Impacts of El Niño and La Niña on the cycle of the East Asian winter and summer monsoon. Chin J Atmos Sci (in Chinese) 26:595–610
5. Chen Z, Wen Z, Wu R, Lin X, Wang J (2016) Relative importance of tropical SST anomalies in maintaining the western North Pacific anomalous anticyclone during El Niño to La Niña transition years. Clim Dyn 46:1027–1041. https://doi.org/10.1007/s00382-015-2630-1
6. Chen Z, Wen Z, Wu R, Du Y (2017) Roles of tropical SST anomalies in modulating the western north Pacific anomalous cyclone during strong La Niña decaying years. Clim Dyn 49:633–647. https://doi.org/10.1007/s00382-016-3364-4
7. Chen Z, Du Y, Wen Z, Wu R, Wang C (2018) Indo-Pacific climate during the decaying phase of the 2015/16 El Niño: Role of southeast tropical Indian Ocean warming. Clim Dyn 50:4707–4719. https://doi.org/10.1007/s00382-017-3899-z
8. Chen Z, Du Y, Wen Z, Wu R, Xie SP (2019) Evolution of South Tropical Indian Ocean Warming and the Climatic Impacts Following Strong El Nino Events. J Clim 32:7329–7347. https://doi.org/10.1175/JCLI-D-18-0704.1
9. Chiang JC, Sobel AH (2002) Tropical tropospheric temperature variations caused by ENSO and their influence on the remote tropical climate. J Clim 15.18: 2616–2631. https://doi.org/10.1175/1520-0442(2002)015<2616:TTTVCB>2.0.CO;2
10. Chowdary JS, Attada R, Attada R, Lee JY et al (2014) Seasonal prediction of distinct climate anomalies in summer 2010 over the tropical Indian Ocean and South Asia. J Meteorol Soc Jpn

921:1–16. https://doi.org/10.2151/jmsj.2014-101

11. Ding YH (1992) Summer monsoon rainfalls in China. J Meteorol Soc Jpn 70:373–396. https://doi.org/10.2151/jmsj1965.70.1B_373
12. Ding YH, Sun Y (2001) A study on anomalous activities of East Asian summer monsoon during 1999. J Meteorol Soc Jpn 79:6: 1119–1137. https://doi.org/10.2151/jmsj.79.1119
13. Ding YH (2007) The variability of the Asian summer monsoon. J Meteorol Soc Jpn 85:21–54. https://doi.org/10.2151/jmsj.85B.21
14. Ding YH, Wang ZY (2008) A study of rainy seasons in China. Meteorol Atmos Phys 100(1):121–138. https://doi.org/10.1007/s00703-008-0299-2
15. Ding YH, Liu YY, Hu ZZ (2021) The Record-breaking Meiyu in 2020 and Associated Atmospheric Circulation and Tropical SST Anomalies. Adv Atmos Sci 1–14. https://doi.org/10.1007/s00376-021-0361-2
16. Du Y, Xie SP, Huang G (2009) Role of air–sea interaction in the long persistence of El Niño–induced north Indian Ocean warming. J Clim 22.8:2023–2038. https://doi.org/10.1175/2008JCLI2590.1
17. Hersbach H, Bell B, Berrisford P, Biavati G, Horányi A, Muñoz Sabater J, Nicolas J, Peubey C, Radu R, Rozum I, Schepers D, Simmons A, Soci C, Dee D, Thépaut JN (2019) ERA5 monthly averaged data on pressure levels from 1979 to present. Copernicus Climate Change Service (C3S) Climate Data Store (CDS). https://doi.org/ 10.24381/cds.6860a573
18. Hersbach H, Bell B, Berrisford P, Biavati G, Horányi A, Muñoz Sabater J, Nicolas J, Peubey C, Radu R, Rozum I, Schepers D, Simmons A, Soci C, Dee D, Thépaut JN (2019) ERA5 monthly averaged data on single levels from 1979 to present Copernicus Climate. Change Service (C3S) Climate Data Store (CDS). https://doi.org/10.24381/cds.f17050d7
19. Huang G, Hu K, Xie SP (2010) Strengthening of tropical Indian Ocean teleconnection to the northwest Pacific since the mid-1970s: An atmospheric GCM study. J Clim 23.19:5294–5304. https://doi.org/10.1175/2010JCLI3577.1
20. Huang R, Sun F (1992) Impact of the tropical western Pacific on the East Asian summer monsoon. J Meteorol Soc Jpn 70:213–256. https://doi.org/10.2151/jmsj1965.70.1B_243
21. Klein SA, Soden BJ, Lau N-C (1999) Remote sea surface temperature variations during ENSO: evidence for a tropical atmospheric bridge. J Clim 12:917–932. https://doi.org/10.1175/1520-0442(1999)012<0917:RSSTVD>2.0.CO;2
22. Kosaka Yu, Xie SP, Lau NC, Vecchi GA (2013) Origin of seasonal predictability for summer climate over the Northwestern Pacific. Proceedings of the National Academy of Sciences 110.19: 7574–7579. https://doi.org/10.1073/pnas.1215582110
23. Lu RY (2001) Interannual variability of the summertime North Pacific subtropical high and its relation to atmospheric convection over the warm pool. J Meteorol Soc Jpn 79.3:771–783. https://doi.org/10.2151/jmsj.79.771
24. Lu R, Dong B (2001) Westward extension of North Pacific subtropical high in summer. J Meteorol Soc Jpn 79:1229–1241. https://doi.org/10.2151/jmsj.79.1229

25. Gao C, Chen H, Li G et al (2019) Land–atmosphere interaction over the Indo-China Peninsula during spring and its effect on the following summer climate over the Yangtze River basin. Clim Dyn 53:6181–6198. https://doi.org/10.1007/s00382-019-04922-x
26. Ninomiya K, Kobayashi C (1998) Precipitation and moisture balance of the Asian summer monsoon in 1991 Part I: Precipitation and major circulation systems. J Meteorol Soc Jpn 76.6:855–877. https://doi.org/10.2151/jmsj1965.76.6_855
27. Pai DS, Sreejith OP (2011) Global and Regional circulation anomalies: A Report. IMD Met Monograph No Synoptic Meteorology 10:63–78
28. Reynolds R W, Rayner NA, Smith TM, Stokes DC, Wang W (2002) An improved in situ and satellite SST analysis for climate. J Clim 15.13:1609–1625. https://doi.org/10.1175/1520-0442(2002)015<1609:AIISAS>2.0.CO;2
29. Richter I, Xie SP (2010) Moisture transport from the Atlantic to the Pacific basin and its response to North Atlantic cooling and global warming. Clim Dyn 35.2:551–566. https://doi.org/10.1007/s00382-009-0708-3
30. Sampe T, Xie SP (2010) Large-scale dynamics of the meiyu-baiu rainband: Environmental forcing by the westerly jet. J Clim 23.1:113–134. https://doi.org/10.1175/2009JCLI3128.1
31. Sherwood SC, Roca R, Weckwerth TM, Andronova NG (2010) Tropospheric water vapor, convection, and climate. Rev Geophys 48.2. https://doi.org/10.1029/2009RG000301
32. Simmonds I, Bi D, Hope P (1999) Atmospheric water vapor flux and its association with rainfall over China in summer. J Clim 12.5:1353–1367. https://doi.org/10.1175/1520-0442(1999)012<1353:AWVFAI>2.0.CO;2
33. Takaya Y, Ishikawa I, Kobayashi C, Endo H, Ose T (2020) Enhanced Meiyu-Baiu rainfall in early summer 2020: Aftermath of the 2019 super IOD event. Geophys Res Lett 47.22: e 2020GL090671
. https://doi.org/10.1029/2020GL090671
34. Trenberth KE (1991) Climate diagnostics from global analyses: conservation of mass in ECMWF analyses. J Clim 4:707–722. https://doi.org/10.1175/1520-0442(1991)004<0707:CDFGAC>2.0.CO;2
35. Trenberth KE, Dai A, Rasmussen RM, Parsons DB (2003) The changing character of precipitation. Bull Am Meteor Soc 84:9:1205–1218. https://doi.org/10.1175/BAMS-84-9-1205
36. Wang B, Xiang B, Lee JY(2013) Subtropical high predictability establishes a promising way for monsoon and tropical storm predictions. Proceedings of the National Academy of Sciences 110.8: 2718–2722. https://doi.org/10.1073/pnas.1214626110
37. Wei K, Ouyang C, Duan H, Li Y, Chen M, Ma J, An H, Zhou S (2020) Reflections on the catastrophic 2020 Yangtze River Basin flooding in southern China. The Innovation 1.2:100038. https://doi.org/10.1016/j.xinn.2020.100038
38. Wu R, Hu ZZ, Kirtman BP (2003) Evolution of ENSO-related precipitation anomalies in East Asia and the processes. J Clim 16:3742–3758. https://doi.org/10.1175/1520-0442(2003)016<3742:EOERAI>2.0.CO;2

39. Xie SP, Hu K, Hafner J, Tokinaga H, Du Y, Huang G, Sampe T (2009) Indian Ocean capacitor effect on Indo–western Pacific climate during the summer following El Niño. J Clim 22.3:730–747. https://doi.org/10.1175/2008JCLI2544.1
40. Xie SP, Kosaka Y, Du Y, Hu K, Chowdary JS, Huang G (2016) Indo-western Pacific Ocean capacitor and coherent climate anomalies in post-ENSO summer: A review. Adv Atmos Sci 33.4:411–432. https://doi.org/10.1007/s00376-015-5192-6
41. Yang J, Liu Q, Xie SP, Liu Z, Wu L (2007) Impact of the Indian Ocean SST basin mode on the Asian summer monsoon. Geophys Res Lett 34:2. https://doi.org/10.1029/2006GL028571
42. Zheng JY, Wang CZ (2021) Influences of three oceans on record-breaking rainfall over the Yangtze River Valley in June 2020. Sci China Earth Sci 10. https://doi.org/10.1007/s11430-020-9758-9
43. Zhou TJ, Yu RC (2005) Atmospheric water vapor transport associated with typical anomalous summer rainfall patterns in China. J Geophys Res Atmos 110.D8. https://doi.org/10.1029/2004JD005413
44. Zhou ZQ, Xie SP, Zhang R (2021) Historic Yangtze flooding of 2020 tied to extreme Indian Ocean conditions. Proceedings of the National Academy of Sciences 118.12. https://doi.org/10.1073/pnas.2022255118
45. Zhu Y, Wang H, Zhou W et al (2011) Recent changes in the summer precipitation pattern in East China and the background circulation. Clim Dyn 367 8:1463–1473. https://doi.org/10.1007/s00382-010-0852-9

Figures

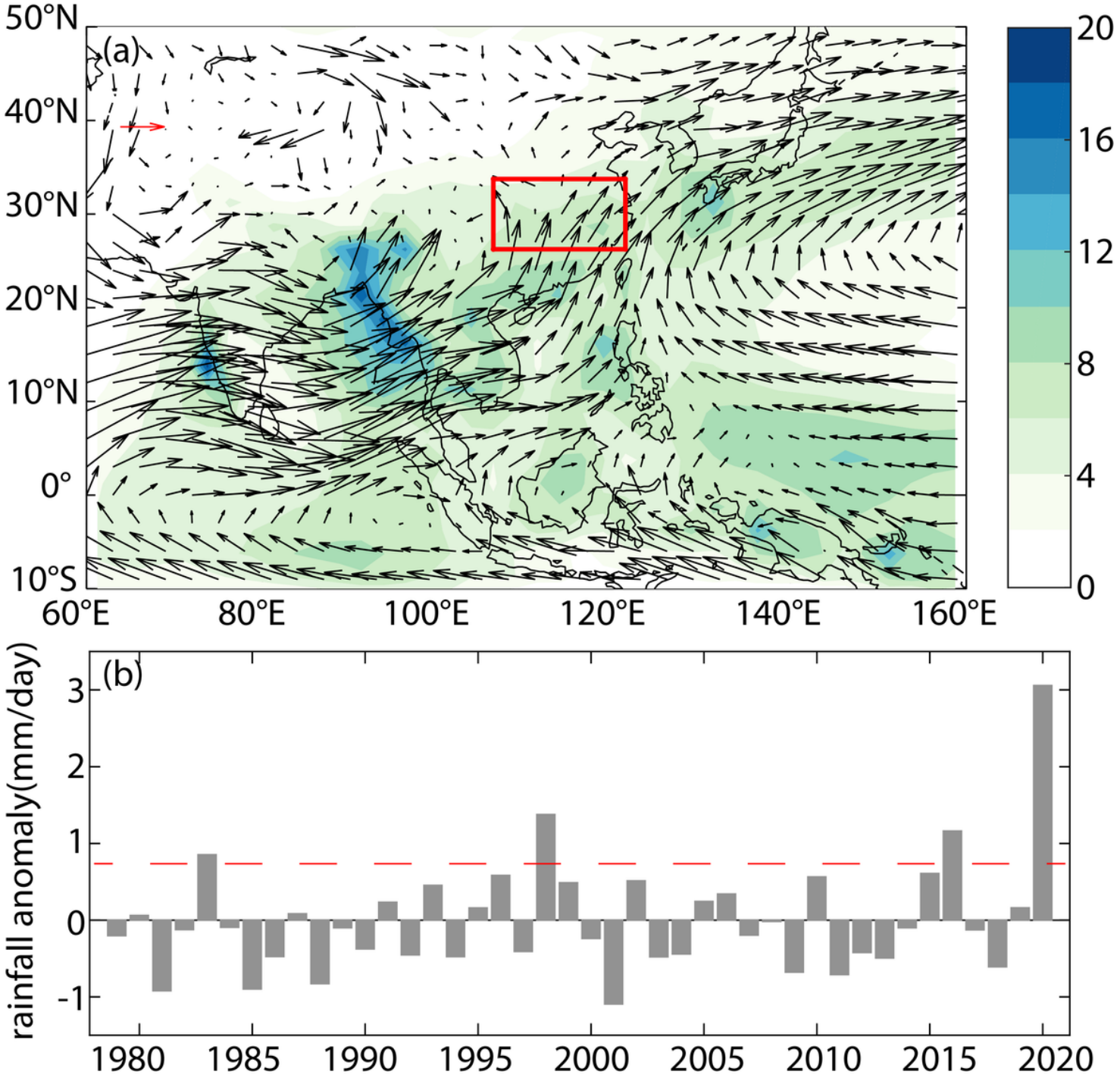

Figure 1

a Climatology of 850 hPa wind (vectors, unit: m/s) and precipitation (shading, unit: mm/day) in MJJ. The red box denotes the central China region. b Time series of rainfall anomalies of the central China region (gray bars, unit: mm/day), red dashed line indicates the one standard deviation of rainfall anomalies

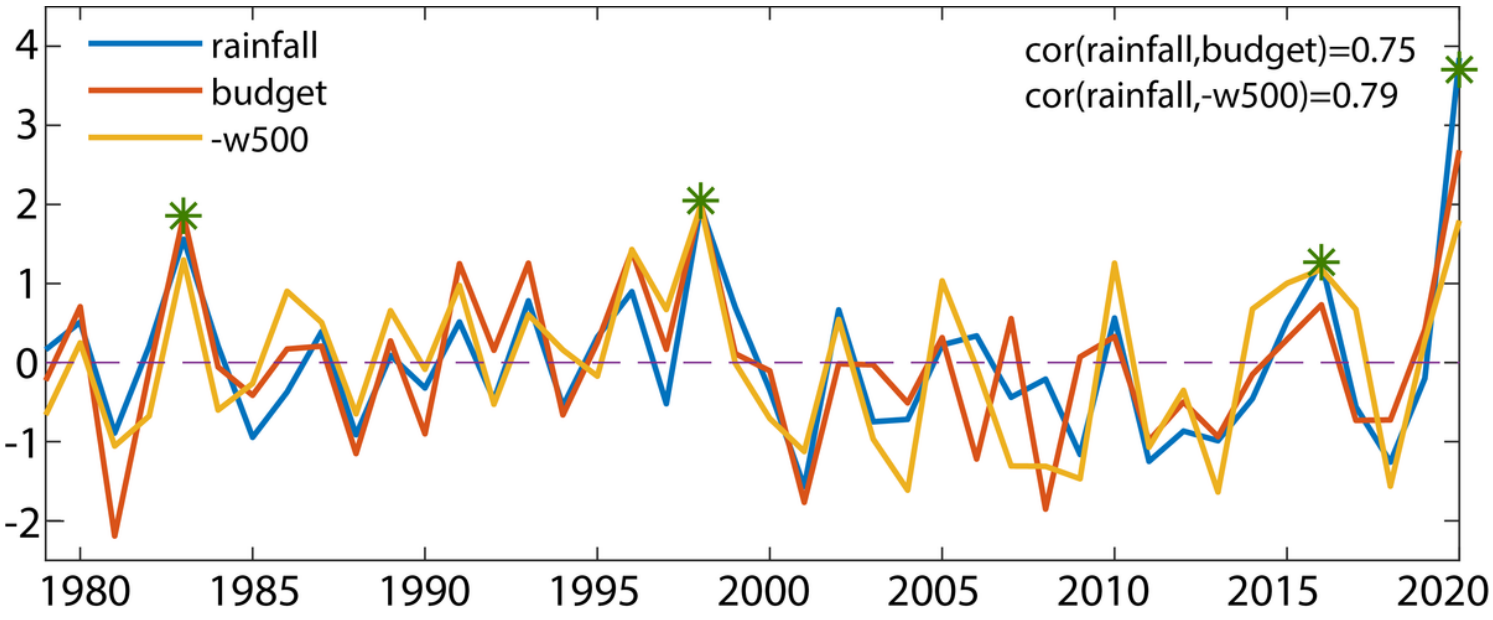

Figure 2

Normalized time series of the average mean of rainfall (blue line), net water vapor budget (orange line), and p-velocity on 500 hPa (multiplied by −1, yellow line) anomalies on central China during MJJ. The extreme rainfall events are tagged by green star markers

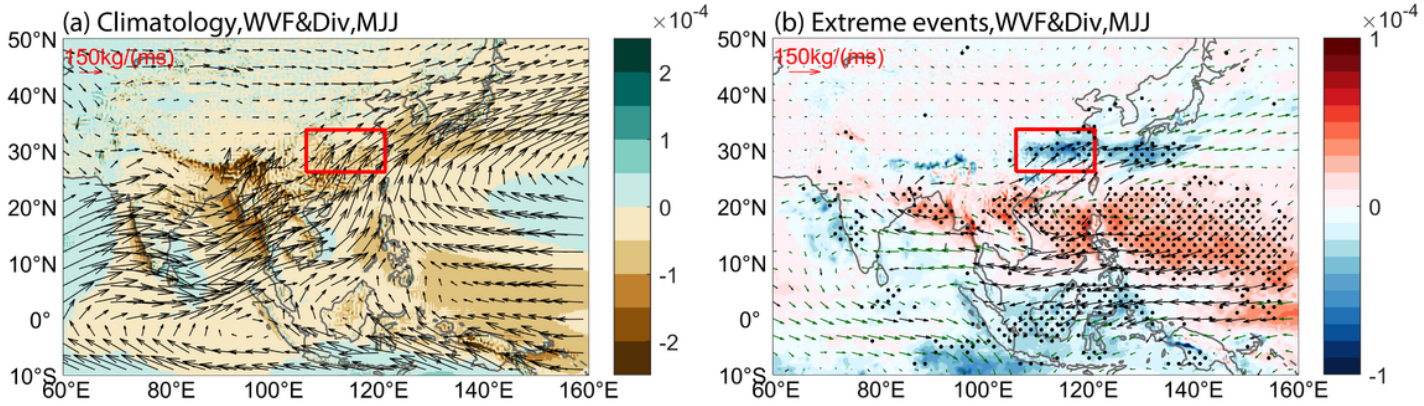

Figure 3

a Climatology of vertical integral of water vapor flux (WVF) (vectors, unit: kg/(m·s)) and divergence (shading, unit: kg/(m2·s)). b Composite of vertical integral of water vapor flux (WVF) (vectors, unit: kg/(m·s)) and divergence (shading, unit: kg/(m2·s)) anomalies in four extreme rainfall events (i.e., 1983, 1998, 2016, 2020). The red box denotes the central China region. The stippled areas denote the divergence anomalies are significant at 95 % confidence level according to student's t test. The black vectors denote the WVF anomalies are significant at 95 % confidence level

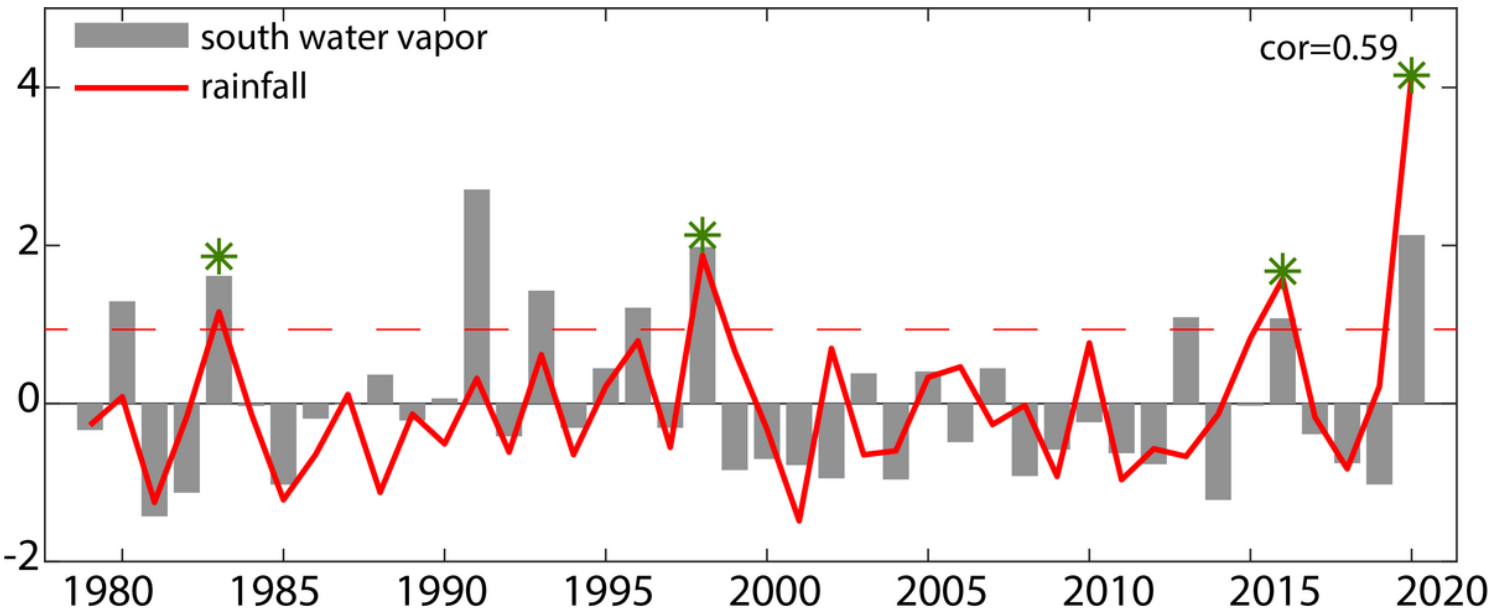

Figure 4

Normalized time series of water vapor anomalies through the south boundary and rainfall anomalies over the central China during MJJ, red dashed line indicates the one standard deviation of south water vapor anomalies, the extreme rainfall events are tagged by green star markers

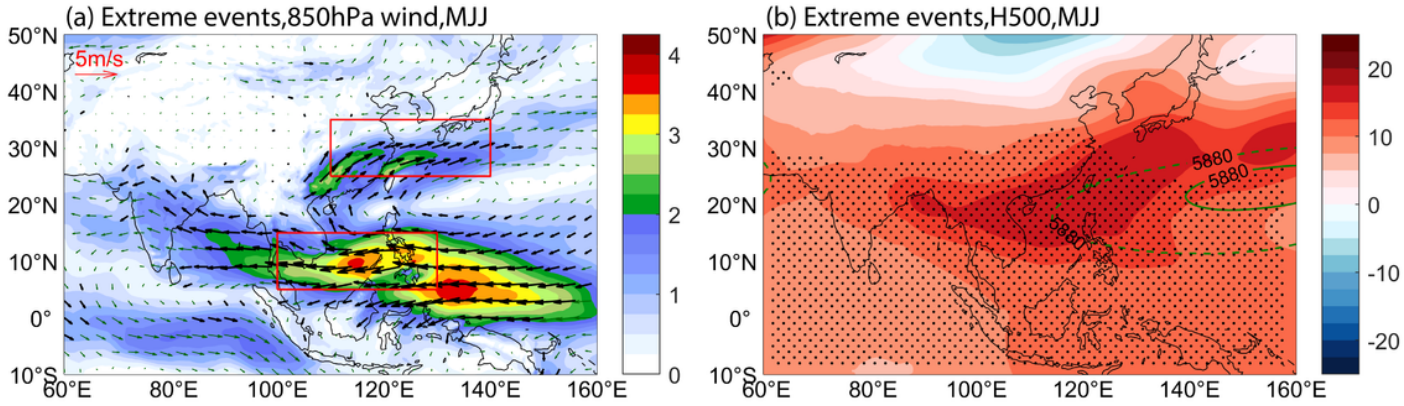

Figure 5

a Composite of 850 hPa wind anomalies (vectors, unit: m/s) in four extreme rainfall events, the shading denotes the wind anomaly intensity, the black vectors denote the wind anomalies is significant at 95 % confidence level according to student's t test, the two red boxes denote the regions to define WNPAC index. b Composite of 500 hPa geopotential height anomalies (shading, unit: gpm) in four extreme rainfall events, the solid and dashed green lines (the 5880 gpm contour lines) represent the main body of

the WPSH in climate mean and extreme events, respectively. The stippled areas denote the geopotential height anomalies are significant at 95 % confidence level according to student's t test

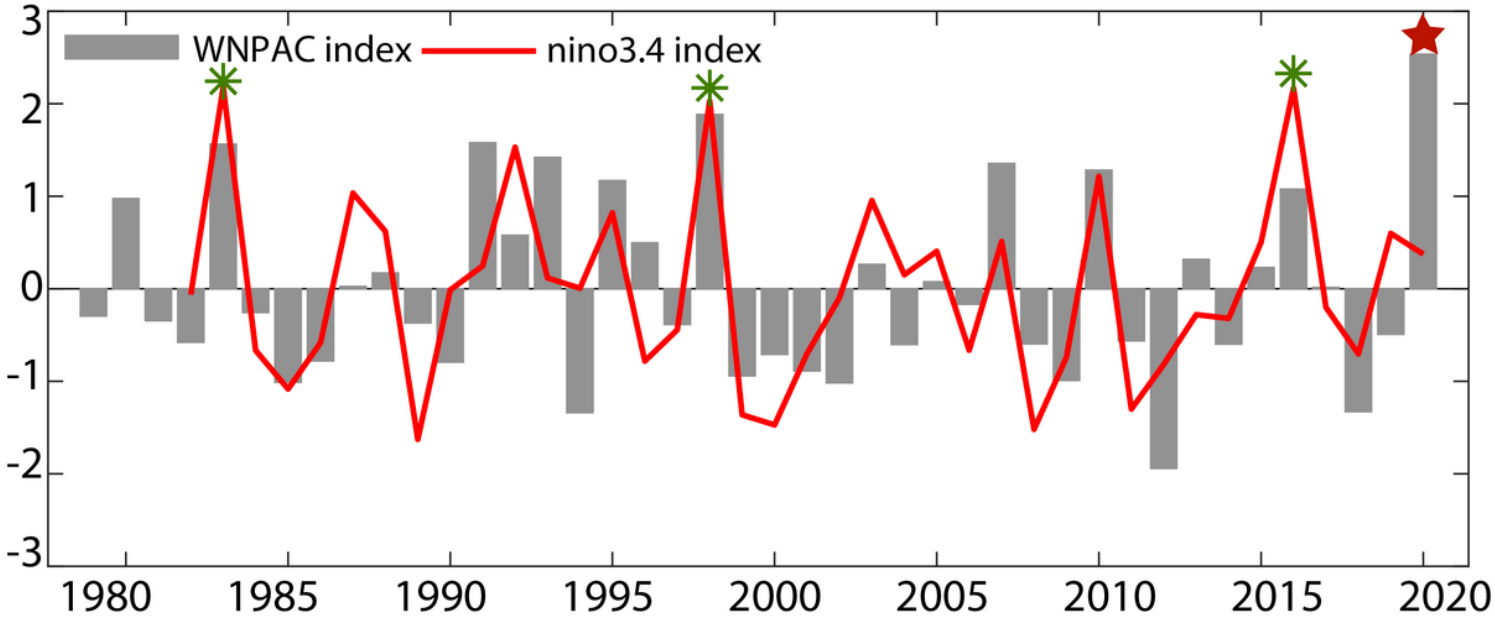

Figure 6

Normalized MJJ WNPAC index and D(-1)JF(0) Niño3.4 index, the numerals '-1' and '0' signify the previous and current year, respectively. The WNPAC index is defined by the difference of 850 hPa zonal wind between a southern region (100°E-130°E, 5°N-15°N) and a northern region (110°E-140°E, 25°N-35°N), which is presented in Fig.5. 2020 extreme rainfall event is tagged by red pentagram marker, other three events following strong El Niño events are tagged by green star markers

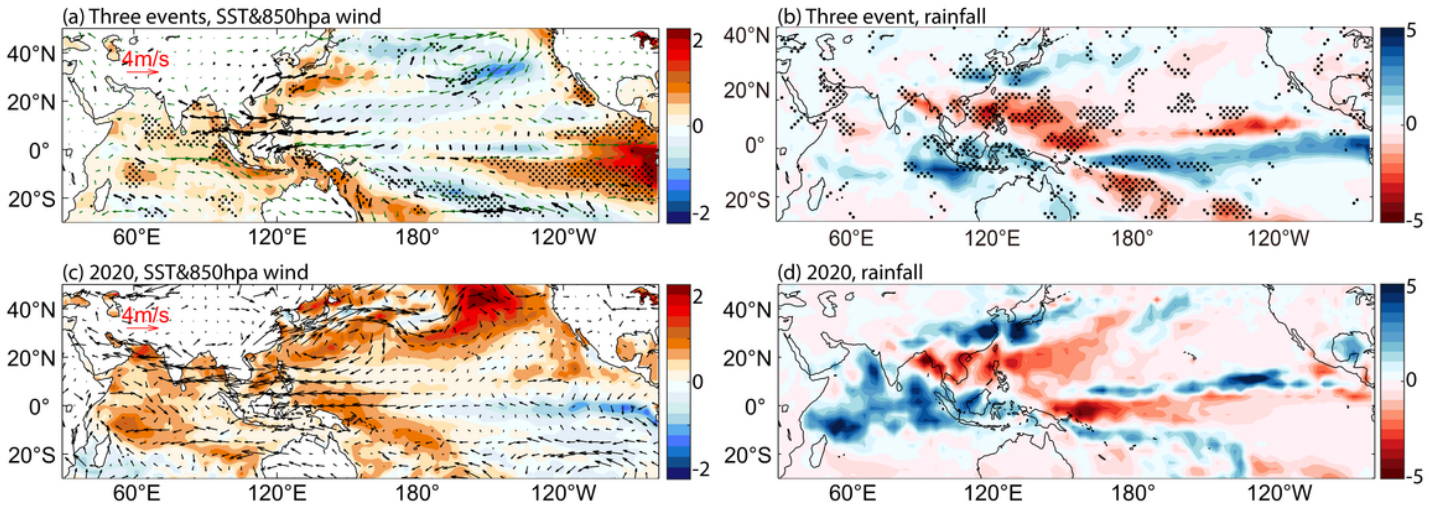

Figure 7

MJJ SST (shading, unit:℃) and 850-hPa wind anomalies (vectors, unit: m/s) during three events following strong El Niño events (1983, 1998, 2016) (a) and 2020 (c), MJJ rainfall anomalies (shading, unit: ℃) during strong El Nino years (1983, 1998, 2016) (b) and 2020 (d). In a, the stippled areas denote the SST anomalies are significant at 95 % confidence level according to student's t test, the black vectors denote the wind anomalies are significant at 95 % confidence level according to student's t test. In b, the stippled areas denote the rainfall anomalies are significant at 95 % confidence level according to student's t test

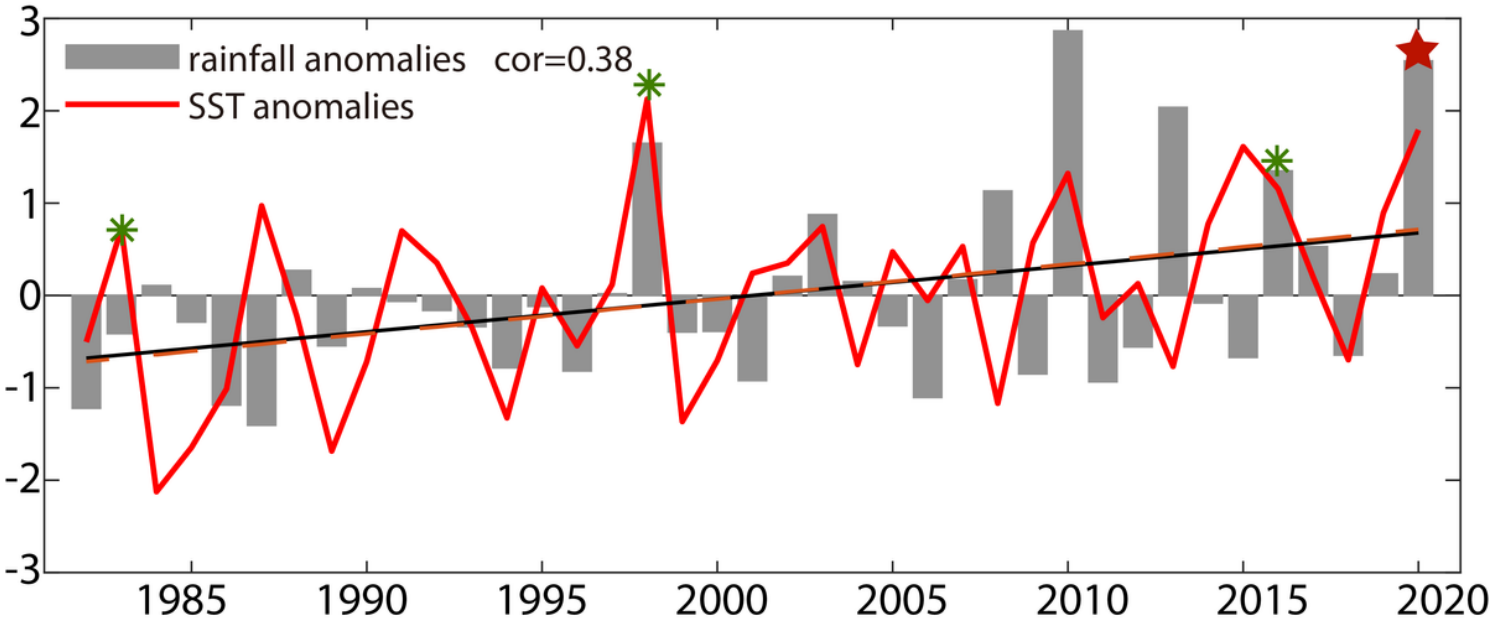

Figure 8

Normalized time series of rainfall and SST anomalies in the tropical Indian Ocean (TIO, 15°S-15°N, 45°E-110°E). 2020 extreme rainfall event is tagged by red pentagram marker, other three events following strong El Niño events are tagged by green star markers. Black solid and orange dashed lines are the linear trends of normalized rainfall and SST anomalies, respectively

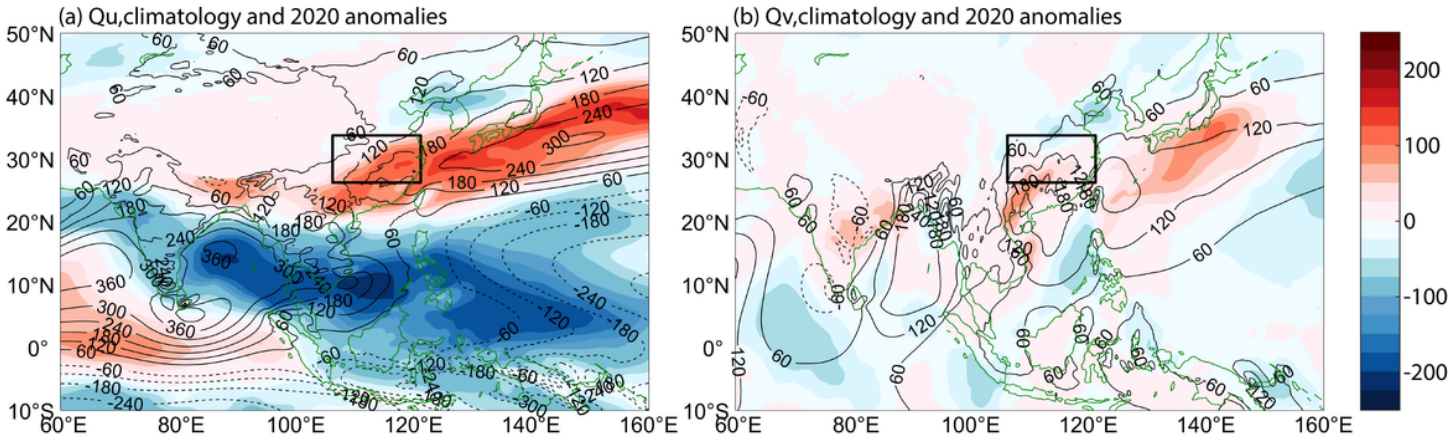

Figure 9

Vertical integral of (a) zonal and (b) meridional water vapor flux (unit: kg/(m·s)). The contours and shading represent the climatology and anomaly in 2020, respectively

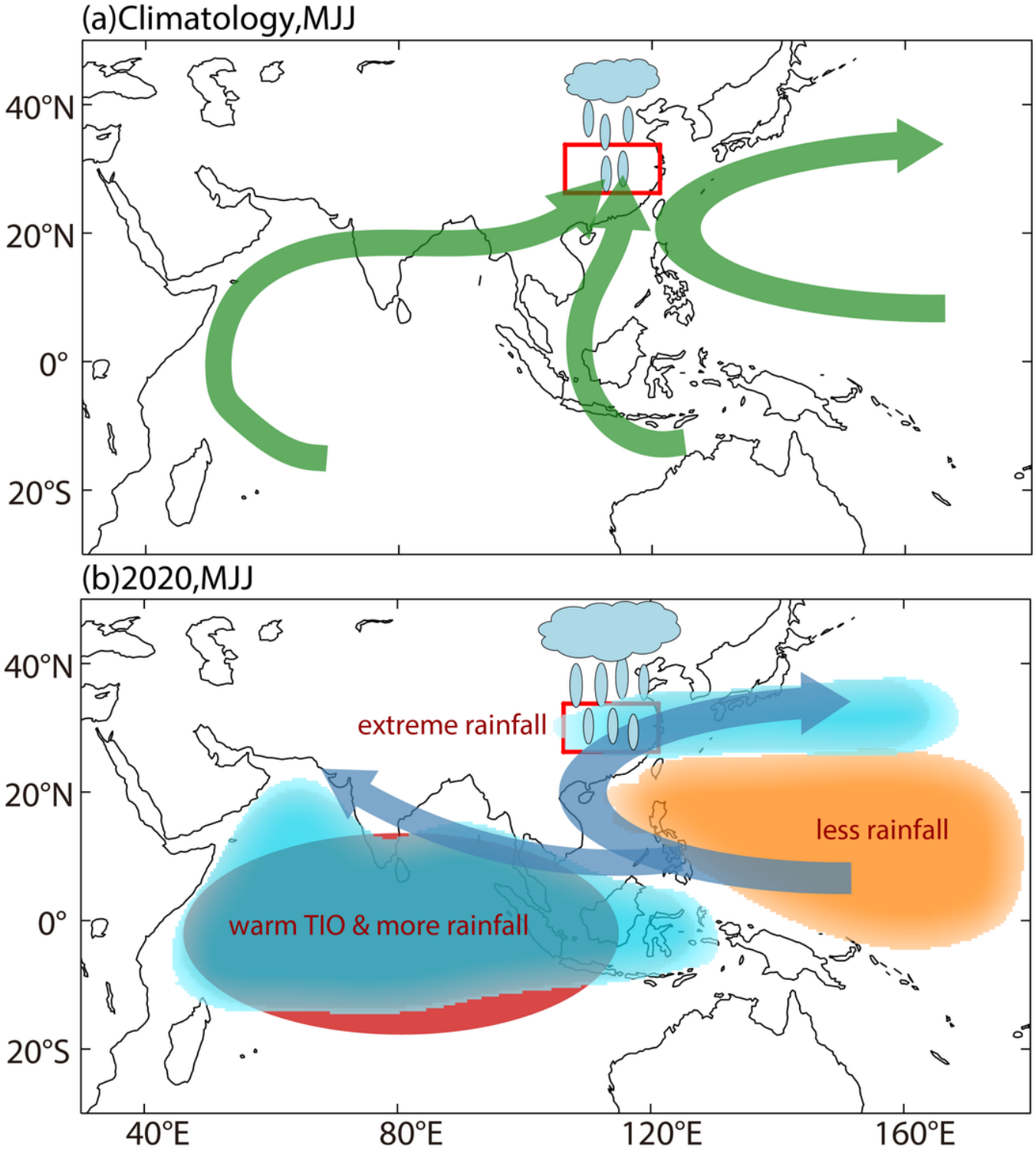

Figure 10

Schematic representations of climate mean state and 2020, respectively. a Climate mean water vapor transport path (green arrows) in MJJ. b anomalous water vapor transport (blue arrows), red circles denote SST warming, yellow (blue) shading denote less (more) rainfall in 2020 MJJ